Establishment and Comprehensive Characterization of a Novel Preclinical Platform of Metastatic Retinoblastoma for Therapeutic Developments

Santiago Zugbi,[1,2] Rosario Aschero,[2–4] Daiana Ganiewich,[5] María B. Cancela,[1,2] Ursula Winter,[1,3] Daniela Ottaviani,[6] Claudia Sampor,[7] Milagros Dinardi,[1] Ana V. Torbidoni,[1,2] Marcela Mena,[5] Leire Balaguer-Lluna,[4] Gabriela Lamas,[3] Mariana Sgroi,[8] Eduardo Lagomarsino,[9] Fabiana Lubieniecki,[3] Adriana Fandiño,[8] François Radvanyi,[6] David H. Abramson,[10] Osvaldo Podhajcer,[2,5] Andrea S. Llera,[2,5] Eduardo G. Cafferata,[2,5] Guillermo Chantada,[2,4] Angel M. Carcaboso,[4] and Paula Schaiquevich[1,2]

[1]Innovative Treatments Unit, Hospital de Pediatría JP Garrahan, Buenos Aires, Argentina
[2]National Scientific and Technical Research Council, CONICET, Buenos Aires, Argentina
[3]Pathology Service, Hospital de Pediatría JP Garrahan, Buenos Aires, Argentina
[4]SJD Pediatric Cancer Center Barcelona, Hospital Sant Joan de Deu, Institut de Recerca Sant Joan de Deu, Barcelona, Spain
[5]Laboratory of Molecular and Cellular Therapy, Instituto Leloir – Instituto de Investigaciones Bioquímicas de Buenos Aires (IIBBA), Buenos Aires, Argentina
[6]Institut Curie; PSL Research University, Centre National de la Recherche Scientifique (CNRS); Equipe Ligue contre le cancer, Paris, France
[7]Hematology-Oncology Service, Hospital de Pediatría JP Garrahan, Buenos Aires, Argentina
[8]Ophthalmology Service, Hospital de Pediatría JP Garrahan, Buenos Aires, Argentina
[9]Pharmacy Service, Hospital de Pediatría JP Garrahan, Buenos Aires, Argentina
[10]Ophthalmic Oncology Service, Memorial Sloan Kettering Cancer Center, New York, New York, United States

Correspondence: Paula Schaiquevich, Combate de los pozos 1881, CP1245, CABA, Buenos Aires, Argentina; paulas@conicet.gov.ar.

Received: September 25, 2023
Accepted: November 20, 2023
Published: December 20, 2023

Citation: Zugbi S, Aschero R, Ganiewich D, et al. Establishment and comprehensive characterization of a novel preclinical platform of metastatic retinoblastoma for therapeutic developments. *Invest Ophthalmol Vis Sci.* 2023;64(15):27. https://doi.org/10.1167/iovs.64.15.27

Purpose. Although there have been improvements in the management of metastatic retinoblastoma, most patients do not survive, and all patients suffer from multiple short- and long-term treatment toxicities. Reliable and informative models to assist clinicians are needed. Thus we developed and comprehensively characterized a novel preclinical platform of primary cell cultures and xenograft models of metastatic retinoblastoma to provide insights into the molecular biology underlying metastases and to perform drug screening for the identification of hit candidates with the highest potential for clinical translation.

Methods. Orbital tumor, bone marrow, cerebrospinal fluid, and lymph node tumor infiltration specimens were obtained from seven patients with metastatic retinoblastoma at diagnosis, disease progression, or relapse. Tumor specimens were engrafted in immunodeficient animals, and primary cell lines were established. Genomic, immunohistochemical/immunocytochemical, and pharmacological analysis were performed.

Results. We successfully established five primary cell lines: two derived from leptomeningeal, two from orbital, and one from lymph node tumor dissemination. After the intravitreal or intraventricular inoculation of these cells, we established cell-derived xenograft models. Both primary cell lines and xenografts accurately retained the histological and genomic features of the tumors from which they were derived and faithfully recapitulated the dissemination patterns and pharmacological sensitivity observed in the matched patients.

Conclusions. Ours is an innovative and thoroughly characterized preclinical platform of metastatic retinoblastoma developed for the understanding of tumor biology of this highly aggressive tumor and has the potential to identify drug candidates to treat patients who currently lack effective treatment options.

Keywords: metastatic retinoblastoma, xenografts, drug sensitivity, genomics, primary cell lines

Copyright 2023 The Authors

This work is licensed under a Creative Commons Attribution-NonCommercial-NoDerivatives 4.0 International License.

Downloaded from hwmaint.iovs.org on 04/26/2024

Retinoblastoma is the most common primary neoplasm of the eye and among the six index tumors of the World Health Organization Global Initiative for childhood cancer. With timely diagnosis, retinoblastoma is highly curable in high-income patients who undergo enucleation or receive state-of-the art treatments for eye preservation.[1] However, a profound inequality exists for children from middle- and low-income countries (LMIC), with up to 50% of them dying of metastatic disease.[2–4]

Highly intensive treatments may result in benefits for patients with metastatic disease but the notable toxicity and limited availability of resources for stem cell transplantation for consolidation limit its widespread implementation in LMIC. Moreover, patients with central nervous system (CNS) involvement invariably succumb to the disease despite chemotherapy intensification.[5]

Certain genomic alterations may contribute to the metastatic pattern. For instance, there is a higher frequency of atypical copy number alterations in chromosome 11q, 17q, and 19q in patients with extraocular disease compared to intraocular cases.[6] In this context, a comprehensive study revealed that tumors molecularly and histologically classified as subtype 2 that harbor *MYCN* amplification, *BCOR* mutations, and segmental chromosome alterations have a higher frequency of metastasis.[7] The prominent role of *MYCN* alterations in metastatic retinoblastoma was also evident in a series of patients with *MYCN* amplification who lacked *RB1* aberrations ($RB1^{+/+}$ $MYCN_{ampl}$) that were unresponsive to intensive treatment.[8] Whether these genomic alterations are more frequently found in LMIC patients because of late diagnosis or other contributing factors is still unknown.

To study the molecular mechanisms of tumor dissemination and risk factors and ultimately to develop more effective treatments that increase overall survival, preclinical models are urgently needed. The establishment of preclinical models for research relies on the availability of institutional programs capable of processing fresh patient samples. However, almost all children with metastatic retinoblastoma live in LMIC where insufficient human training and low economic resources have hindered advancements in research.[9] Although several xenograft models of pediatric tumors have been established and comprehensively characterized,[10–16] primary cell cultures and xenografts derived from metastases are strongly underrepresented. Anecdotal reports on the establishment of cell cultures from metastases by Japanese researchers and isolated patient-derived xenograft (PDX) models of retinoblastoma with regional orbital extension are available, although none involve CNS disease.[11,16] In this work, we present an innovative preclinical platform that encompasses the biological heterogeneity of metastatic retinoblastoma, which was developed to extend our understanding on the biology and tumorigenesis of metastatic tumors and for drug screening purposes in an effort to identify the therapeutic potential to cure patients with metastatic disease.

Material and Methods

The present study followed the tenets of the Declaration of Helsinki and was approved by the Institutional Review Board at Hospital de Pediatria JP Garrahan (protocol no. 838) for prospective procurement of biological material for genomic studies and establishment of cell cultures from the primary tumor and the metastatic sites. Written informed consent was obtained from parents.

Animal studies were conducted in compliance with the Statement for the Use of Animals in Ophthalmic and Vision Research of the Association for Research in Vision and Ophthalmology. Approval was granted by the Institutional Animal Care and Use Committee of Fundación Instituto Leloir, Argentina (protocol no. 2019-069) and Hospital Sant Joan de Déu, Spain (protocol 135/11).

Patients were classified according to the International Retinoblastoma Staging System (IRSS).[17] Diagnostic workup to establish disease extension included ocular examination under anesthesia, imaging (computed tomography or magnetic resonance imaging) of the head including the orbit, bone scintigraphy (only symptomatic patients), lumbar puncture and cytology and/or real time quantitative polymerase chain reaction (RT-qPCR) analysis for cone-rod homebox transcription factor RNA (CRX), and bilateral bone marrow aspiration and biopsy. We documented orbital and lymph node invasion by fine-needle biopsy in two cases.

Patients

Consecutive patients with metastatic retinoblastoma treated at Hospital JP Garrahan (Argentina) between 2014 and 2019 were included. Four patients initially had intraocular disease of whom two developed metastasis after treatment with systemic chemotherapy, one after systemic chemotherapy and external radiation therapy, and the remaining patient after enucleation without adjuvant chemotherapy (Table). Additional data of some of the enrolled patients have been recently described.[6,7] The Supplementary material provides a complete description of the clinical presentation, disease course, and treatment plan.

Sample Collection and Heterotopic Tumor Expansion

All specimens were processed within two hours of biopsy and placed in RPMI culture medium (Gibco, Thermo Fisher Scientific, Waltham, MA, USA) for transport. Biopsy specimens were cut into small pieces that were cryopreserved in Synth-a-freeze (Gibco) or snap frozen at −80°C for genomic studies. For heterotopic tumor expansion, we implanted specimens into a subcutaneous space in the flank of six-week-old BALBc nu/nu mice. Cerebrospinal fluid (CSF) specimens were spun in a centrifuge at 2000 rpm for 10 minutes, and the cell pellet was resuspended in chilled Matrigel (BD Bioscience, Franklin Lakes, NJ, USA) and placed on ice until subcutaneous injection into the mouse flank. Further details on heterotopic tumor expansion are provided in Supplementary material.

Establishment and Characterization of Primary Cell Cultures

For tumor models with intraocular origin, we used the Y79 retinoblastoma cell line (ATCC, HTB-18) and primary cells (HPG-RBT-12L) derived from an intraocular tumor after upfront enucleation.[18]

To establish primary cultures from metastatic disease, we mechanically disaggregated freshly excised tumor specimens from human biopsies (orbital tumor) or from xenografts at first engraftment (F0, for CSF and lymph node dissemination in patients) and cultured them in serum-free neural stem-cell medium as described elsewhere.[19–21]

Investigative Ophthalmology & Visual Science

Downloaded from hwmaint.iovs.org on 04/26/2024

Table. Clinical Details of the Metastatic Patients Enrolled in the Protocol and of the Tumor-Derived Preclinical Models

Patient ID	Age at Diagnosis (m)	Time to Metastasis (m)	Laterality	Initial Stage (IRSS)	Treatment	Dissemination Sites	Ultimate Outcome	Preclinical Model ID
1	33	4	Unilateral	I	► Enucleation + GALOP[50] ◄ COG-ARET[5] + IT	CNS	DOD	PDX-CSF-1 HPG-CSF-1*
2	18	5	Bilateral	0	► IAO + Enucleation + EBRT ◄ GALOP + IT + EBRT	Orbit and CNS	DOD	PDX-CSF-0A
3†	19	8	Bilateral	I	► Enucleation ◄ GALOP	Orbit and BM	DOD	—
4	42	Diagnosis	Unilateral	IVb	► COG-ARET + Enucleation	Orbit and CNS	DOD	HPG-RBO-1
5	48	Diagnosis	Unilateral	IVb	► IA + OAC+ IT + Enucleation	Orbit and CNS	DOD	PDX-CSF-0B
6	34	Diagnosis	Unilateral	IVb	► IA + OAC+ IT	CNS	DOD	PDX-CSF-2 HPG-CSF-2
7‡	17	3	Unilateral	0	► CEV + Enucleation ◄ COG-ARET	Orbit and lymph node	DOD	HPG-RBG-1

BM, bone marrow; DOD, dead of disease; EBRT, External beam radiotherapy; IA, intra-arterial chemotherapy; IRSS, International Retinoblastoma Staging System; IT, intrathecal topotecan (0.5 mg/dose); OAC, ophthalmic artery chemotherapy; ►, treatment received at disease diagnosis; ◄, treatment received after relapse; CEV, carboplatin (500 mg/m^2/day), etoposide (100 mg/m^2/day), and vincristine (1.5 mg/m^2/day).

For patients 1, 2, 4, and 6, bone marrow samples were collected and identified as negative by CRX mRNA molecular analysis. In all cases, peripheral blood was obtained for germline DNA analysis.

* Published in reference 47.

† Published in reference 51.

‡ Published in reference 49.

First, cell line authentication was performed by short tandem repeat profiling after genomic DNA extraction. Then, whole exome sequencing (WES) analysis of the xenograft tumors and primary cell lines was performed. Afterward, mutations and copy number alterations (CNA) were compared between cell lines and tumor-matched specimens.

The cell growth characteristics and doubling time were determined as described in the Supplementary material. To address the pharmacological sensitivity to standard-of-care chemotherapy, we calculated the concentration of the drug that caused a 50% decrease in cell proliferation or the IC50 (full description in Supplementary material).[20]

Mouse Xenografts

PDX refers to the tumors established from patient biopsy specimens without previous culture, as tissue fragments implanted in the mouse flank, or cell pellets isolated from tumor fluids such as the CSF or the bone marrow, dispersed in Matrigel (Corning Life Sciences, Tewksbury, MA, USA) and subcutaneously injected in BALBc nu/nu mice. To generate intravitreal xenografts, 2×10^5 tumor cells resuspended in 2 µL of Matrigel were injected into the posterior segment of both eyes of athymic nude mice.[21,22] Eyes reaching the experimental endpoint, defined as an eye three times the normal size,[23] were enucleated under anesthesia and formalin-fixed and paraffin embedded. When both eyes reached the experimental endpoint, peripheral blood and CSF were collected under anesthesia and the brain, bone marrow, and cervical and axillar lymph nodes were dissected after euthanasia. All samples were processed or snap-frozen at −80°C until determination of CRX mRNA using RT-qPCR.[21,22] Relative expression of CRX mRNA was determined and quantified using the $2^{\Delta\Delta Ct}$ method.[24]

Intracranial xenografts were obtained after the inoculation of 5×10^5 tumor cells in the fourth ventricle of athymic mice (n = 6 per group). The endpoint was reached when the animals achieved a 20% weight loss. Otherwise, two animals of each group were euthanized on days 30 or 45 after tumor inoculation for histological analysis and to quantify the tumor load in the brain and bone marrow by CRX detection using RT-qPCR as described above. All animals were subjected to daily monitoring for general status, ocular tumor growth, and neurological function.

Immunohistochemistry and Immunocytochemistry

The expression of CRX (ab14603; Abcam, Cambridge, MA, USA), synaptophysin (NCL-L-SYNAP-299; Leica BioSystems, Wetzlar, Germany), Arrestin 3 (ARR3, 11100-2-AP; Proteintech, Rosemont, IL, USA), Ki-67 (Ki-67 anti-human clone; Dako, Glostrup, Denmark), and human nuclei antibody (nHi, MAB4383; Merck, Kenilworth, NJ, USA) was tested using conventional automated systems.[21,22]

Genomic Analysis

After DNA extraction from fresh or formalin-fixed and paraffin-embedded tumor tissues, mutation analysis for *RB1* was performed using Sanger DNA sequencing and CNA analysis by multiplex ligation-dependent probe amplification assay (P047-B1 RB1; MRC Holland, Amsterdam, Netherlands).[25] Based on the comparison with calls from a normal cohort and the database of benign copy number variants, CNA greater than 500 kb in size and copy-neutral loss of heterozygosity (LOH) greater than 10 Mb were considered to be abnormal based on the established performance characteristics of the assay.

WES analysis of fresh xenograft, human tissue, and cell samples was performed in an Illumina HiSeq 4000 instrument.[22] Analysis was done using annotation of SNPs and INDELS was done with PecanPIE[26,27] and interpretation was aided by Alamut Software Suite v.2.14 (Interactive Biosoftware, Boston, MA, USA) and Varsome.[28] Somatic CNA analysis from aligned BAM files were obtained using FACETS[29]

Investigative Ophthalmology & Visual Science

Downloaded from hwmaint.iovs.org on 04/26/2024

implemented in the Cancer Genomics Cloud.[30,31] The dbSNP database was used for BAF calculations.[32]

Statistical Analysis

Eye survival was calculated using Kaplan Meier analysis. Between-group comparison of the percentage of tumor dissemination into the different compartments was performed by means of Fisher's exact test using GraphPad Prism. $P < 0.05$ was considered statistically significant.

Results

Seven patients with metastatic retinoblastoma were enrolled in the protocol after identification by the treating oncologists at Hospital JP Garrahan (patients 1, 2, 3, and 6) or after referral from another national or regional clinical center (patients 4, 5, and 7). Three patients presented with metastatic disease at diagnosis and four had extraocular relapse (Table). Three patients had CNS and orbital involvement at diagnosis (patients 4, 5 and 6) and one at relapse (patient 2), one developed hematogenous dissemination as a consequence of poor treatment compliance (patient 3), and one presented with an atypical pattern of massive orbital and lymph node tumor infiltration without CNS metastasis (patient 7).[22] Treatments were administered according to COG-ARET 0321 or tailored to the family context as detailed in Table. None of the patients are alive. In patients 1, 2, and 7 metastatic tumor specimens were collected after chemotherapy whereas patients 3, 4, 5, and 6 were chemotherapy-naïve when specimens for model development were obtained.

Genomic Analysis of Metastatic Tumors

RB1 mutations were identified in all patients except case 7 (Supplementary Table S1). Patients 1, 4, and 5 had somatic mutations classified as likely pathogenic or pathogenic in Varsome with a variant allele frequency >92% for patients 4 and 5 indicative of LOH. This second hit (LOH) was confirmed by CNA analysis (Supplementary Table S1). Variant allele frequency of the *RB1* mutation of the tumor of patient 1 was 35%, and the purity calculated by FACETS was 52% indicating the presence of normal tissue in the analyzed sample. Patients with bilateral tumors (patients 2 and 3) carried heterozygous germline mutations classified as pathogenic. Multiplex ligation-dependent probe amplification assay analysis confirmed complete deletion of the *RB1* gene in the tumor sample of patient 6. In addition to *RB1*, *BCOR* was identified as the most frequently mutated gene in metastatic sites with pathogenic variants found in patients 1, 3, and 6 (Supplementary Table S2).

A total of six specimens from different metastatic sites were analyzed for genomic aberrations. We detected the most frequently reported gains in 1q, 2p (or focal *MYCN* gain/amplification), and 6p in 75%, 83%, and 66% of the samples, respectively, whereas 16q loss was present in 66% of the specimens. Patient 5 was the only case without gain/amplification in chromosome 2p. Supplementary Table S3 contains a complete analysis of CNA. We confirmed that these aberrations harbored genes reported as tumorigenic drivers in retinoblastoma such as *MDM4* and *KIF14* in 1q, *MYCN* in 2p, *DEK* and *E2F3* in 6p, and *CDH11* in 16q.[33]

In Vivo Tumor Expansion of Human Biopsies and Primary Cell Cultures

A schematic representation of sample collection and the establishment of in vitro and in vivo models and the genomic characteristics of each sample are represented in Figure 1. Briefly, all patient specimens except the bone marrow aspirate (patient 3) successfully engrafted as PDX in the flank of immunocompromised animals. The average time from subcutaneous implantation to engraftment was between 2 and 4.5 months, except for the PDX established from the lymph node infiltration of patient 7 that engrafted one month after inoculation.

We established four primary cell cultures; two derived from the first filial generation (F0) of the PDX after inoc-

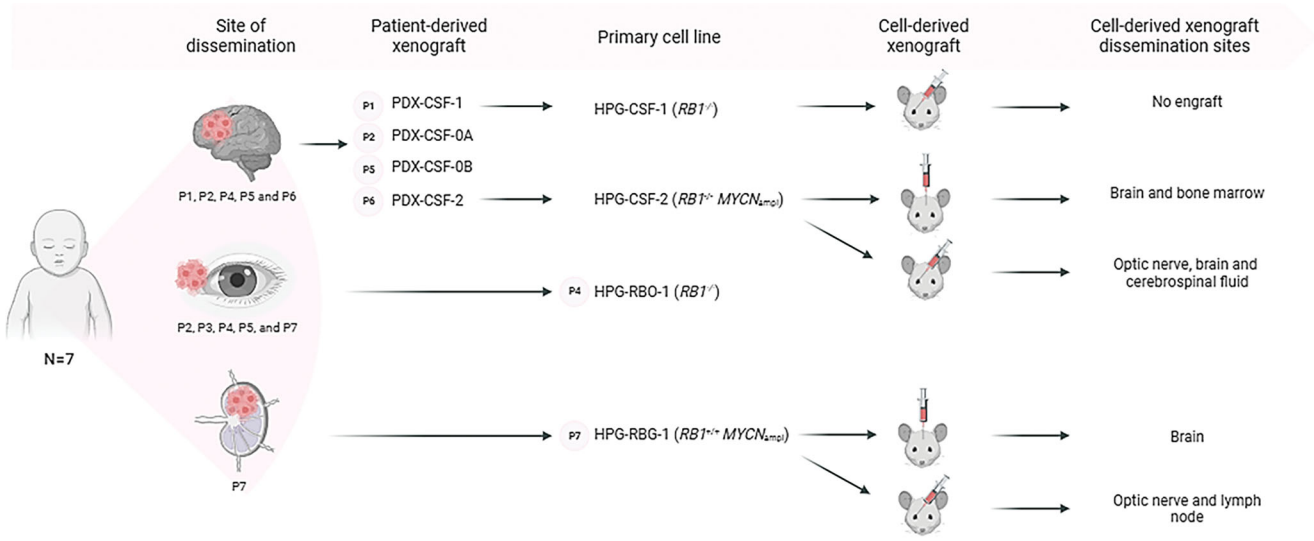

Figure 1. Schematic representation of sample collection and establishment of in vitro and in vivo models of metastatic retinoblastoma. Schematic representation of sample collection from the dissemination sites of each patient and the establishment of PDXs, primary cell lines, and cell-derived xenografts. A description of the main genetic characteristics of each model is included. P, patient; PDX-CSF-0, human tumors engrafted in the animal flank but no cell culture could be established.

Investigative Ophthalmology & Visual Science

Downloaded from hwmaint.iovs.org on 04/26/2024

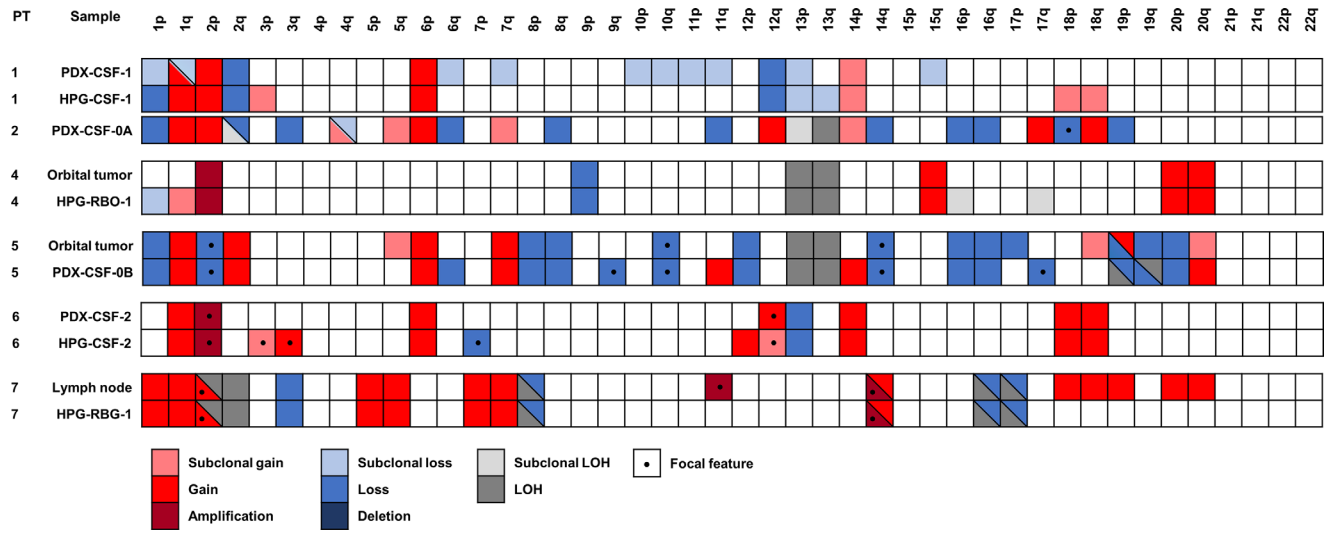

Figure 2. Relevant copy number alterations of the metastatic preclinical models. Somatic copy number alterations of the metastatic preclinical models and the matched tumors. Each row represents an individual sample, and the rectangular boxes correspond to the status of each of the main characteristics. *Boxes* are partitioned if more than one relevant feature coexists. For copy number alterations, gains are shown in *red*, *blue* represents losses, *gray* is for CN-LOH, whereas the intensity of the color shade is proportional to the value of the log-ratio (LRR). In addition, full coloring means the copy number alteration comprises the whole segment (>90% of the arm), whereas a *circle* means part of the segment is altered, and a *star* means it is a focal alteration (<15 genes). The orbital tumors of patients 4 and 5 were considered as a surrogate of the CSF dissemination because they presented with optic nerve and chiasm or hemi-chiasm involvement. CNA of patient 7 lymph node tumor infiltration and the derived model were previously published by Zugbi et al.[22] CN-LOH, copy neutral-loss of heterozygosity; LN, lymph node.

ulation of leptomeningeal dissemination of patients 1 and 6 (HPG-CSF-1 and HPG-CSF-2, respectively), one directly derived from the orbital tumor of patient 4 (HPG-RBO-1), and one derived from the lymph node tumor invasion of patient 7 (HPG-RBG-1) (Table). Attempts to obtain stable cultures from both the CSF dissemination and orbital tumor specimens from patient 5 and orbital tumor tissue from patient 3 were unsuccessful. For the purpose of clarity, the institutional prefix HPG will be omitted hereinafter and primary cell lines will be referred to as CSF-1, CSF-2, RBO-1, and RBG-1.

Genomic Characterization of Primary Cell Lines

Short tandem repeat profiles authenticated the origin of the metastatic cell lines to the matched human extraocular tumors (patients 4 and 7), and the CSF aspirates that were expanded in the flank of mice (patients 1 and 6) as described in Supplementary Table S4. *RB1* mutations identified in the cell lines were the same as those of the tumor of origin. Consistently with the parental tumor that was $RB1^{+/+}$ $MYCN_{ampl}$, RBG-1 cells did not show *RB1* mutations.[22]

Most somatic CNAs, including the known driver alterations, were shared between preclinical models (cells in culture or xenografts) and matched metastatic human tumors (Fig. 2 and full details in Supplementary Table S3). Briefly, for the models derived from the tumor cells of patient 1, both the PDX-CSF-1 tumor and its derived cell line CSF-1 shared gains in 1q, 2p, 6p, 14p and losses in 2q, 12q, 13q (including *RB1*) and a portion of the X chromosome. The orbital metastasis of patient 4 and its derived cell line shared the clonal gain in 2p, with focal amplification of *MYCN*, gains in 15q and chromosome 20, and a loss of 9p and the chromosome 13 LOH that includes *RB1*. For patient 5, both the orbital tumor and the PDX that derived from the leptomeningeal metastasis shared gains in 1q, 6p, 7q, 20q (subclonal in the tumor) and losses in 1p, 2p (focal), 10q (focal), 12p, 19q, 20p, as well as whole chromosomes 8 and 16. The PDX sample from the tumor of patient 6 as well as its derived cell line shared gains in 1q, 2p (with focal *MYCN* amplification), 6p, 12q (subclonal in the cell line), 14p, and chromosome 18, as well as a loss in 13p.

Genomic features of HPG-RBG-1 cells and the matched human tumor from patient 7 were extensively described by Zugbi et al.[22] In short, CNA analysis of this cell line using exome sequencing revealed extensive aneuploid features. These characteristics were confirmed by karyotype studies that also showed homogeneous staining regions and double-minutes typically seen in *MYCN*-amplified cells. We detected a focal high-level (>60×) amplification of *MYCN* in 2p and a high-level amplification (>20) in 14q harboring *OTX2*. No alterations in copy number were seen in the *RB1* gene. WES point mutation analysis revealed a *TP53* mutation (nM_000546.4:c.713G>A, p.[Cys238Tyr]) with an allele frequency of 98% resulting from an LOH in chromosome 17. No point mutations or indels were detected in *RB1*.

Phenotypical Characteristics of Primary Cell Lines

All four primary cell cultures grew as tumorspheres (Supplementary Fig. S1) showing positive staining for Ki67 (proliferative cells), as well as expression of photoreceptor lineage markers CRX and ARR3, and of the neuronal marker synaptophysin (Fig. 3). Phenotypical characteristics of the RBG-1 cell model have been previously reported.[23]

At passages 3 to 4, the four metastatic cell lines showed an exponential growth pattern with an estimated mean (range) doubling time of 2.6 days (2.3–2.9), 2.3 days (2.1–3.3), 2.1 days (1.9–2.4), and 8.6 days (7.5–9.9) for CSF-1,

Investigative Ophthalmology & Visual Science

Downloaded from hwmaint.iovs.org on 04/26/2024

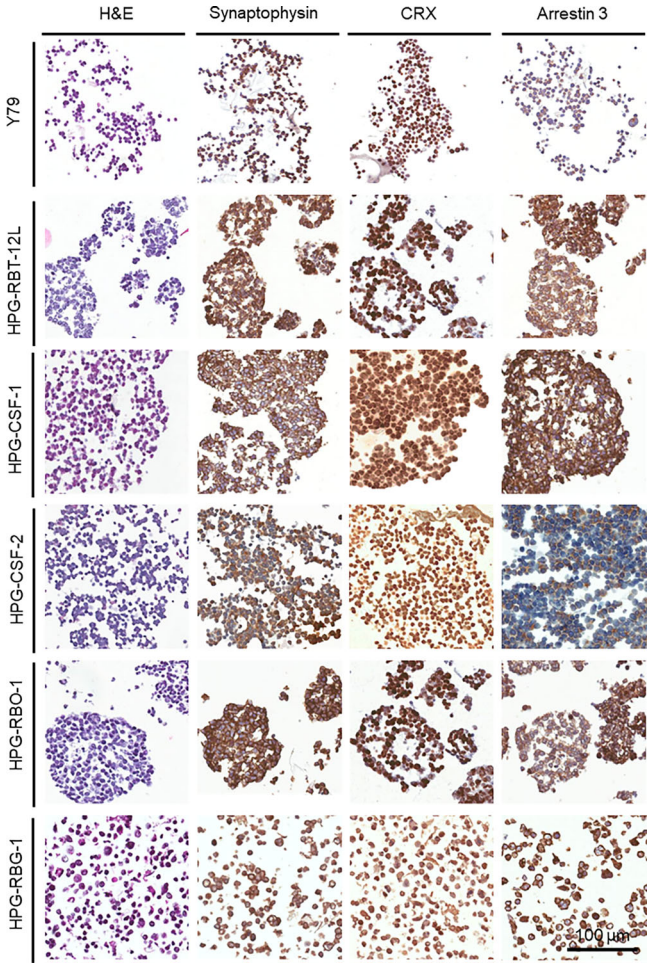

Figure 3. Immunocytochemical characteristics of the primary tumor cell lines. Representative micrographs of each primary cell model and the control cultures HPG-RBT-12L and Y79 are observed for a hematoxylin-eosin staining (×20) and three immunohistochemical stains (×20). Regarding the histological staining, HPG-CSF-2, HPG-RBG-1, and Y79 cells present less compact and irregular neurospheres, whereas HPG-CSF-1, HPG-RBO-1, and HPG-RBT-12L models present compact and homogeneous neurospheres. All cell lines were positive for the marker of neuroectodermal origin synaptophysin and for the specific photoreceptor lineage markers arrestin 3 and CRX. Characteristics of the HPG-RBG-1 cell model were previously reported.[22]

CSF-2, RBG-1, and RBO-1, respectively, whereas RBO-1 cells showed the slowest growth rate (Supplementary Fig. S2).

Pharmacological sensitivity of the cell cultures to standard-of-care chemotherapy is depicted in Figure 4 with the corresponding analysis provided in Supplementary Table S5. Two metastatic primary cells (RBO-1 and RBG-1) were more resistant to topotecan than cells of intraocular origin. For instance, RBG-1 was insensitive to topotecan in the range in which the drug can be solubilized.[22] Although RBO-1 cells were derived from a nontreated patient, they exhibited more resistance to topotecan when compared to intraocular cells. Noteworthy, CSF-2 cells (derived from the CSF of a non-treated patient) demonstrated the highest sensitivity to topotecan with an IC50 of 3 nM ($P < 0.01$, compared to intraocular control cells). Regarding sensitivity to carboplatin, all metastatic cell lines exhibited greater sensitivity than cells of intraocular origin ($P < 0.01$). Finally, all but RBG-1 metastatic cells demonstrated either similar or higher sensitivity to melphalan compared to control cells.

Tumor Engraftment and Dissemination Patterns of Cell-Derived Xenografts of Metastatic Retinoblastoma

All eyes intravitreally injected with CSF-2 and RBG-1 as two representative cell models of leptomeningeal and lymph node dissemination, respectively, developed ocular tumors (see Fig. 1 for workflow). In contrast, CSF-1 cells (leptomeningeal origin) failed to engraft in the mouse eyes. After the appearance of leukocoria (stage 1), eyes showed clear proptosis, localized neovascularization, and total occupation of the eyeball without macroscopic extraocular spread but with distension of the surrounding tissue (stage 2 and 3) as shown in Supplementary Figure S3. Intravitreal xenografts of the control Y79 and RBT-12L cells were associated with a median ocular survival of 35 days (range 21–60) and 51 days (range 35–58), respectively. The median survival of eyes injected with RBG-1 and CSF-2 cells was 29 days (range 20–42) and 47 days (range 43–64), respectively, with the former having the shortest duration (Fig. 5A).

Eyes injected with CSF-2 cells showed undifferentiated tumors that completely infiltrated the ocular structures whereas eyes of RBG-1 xenografts exhibited aggressive histopathological features resembling those of the metastatic tumor of patient 7.[22] Consistent with the absence of macroscopic tumor engraftment, eyes inoculated with CSF-1 cells showed necrosis and calcium deposits without viable tumor cells (Fig. 5B).

Tumor dissemination was detected in 70% and 90% of the evaluated brains for the Y79 and RBT-12L intraocular xenografts, respectively (Supplementary Table S6 and schematic representation in Fig. 1). In the metastatic models, 70% of the brains of the CSF-2 xenografts were positive for retinoblastoma cells. Conversely, none (0%) of the animals intravitreally inoculated with RBG-1 cells developed brain dissemination (Fisher's exact test $P < 0.05$ compared to the percentage of brains of Y79 xenografts with tumor infiltration). Interestingly, the invasive capacity of the CSF-2 cells into the brain also became evident as the tumor load of the xenografts was 20 times higher than that of the Y79 xenografts, a well-established model of CNS tumor infiltration ($P < 0.05$).[21,34] In accordance, these were the only animals that exhibited leptomeningeal infiltration, as 60% of the CSF specimens were positive for retinoblastoma cells (Fisher's exact test $P < 0.05$ compared to the percentage of CSF invasion in Y79 xenografts) (Supplementary Table S6).

In agreement with the low capacity of dissemination into the brain, optic nerves of intravitreal RBG-1 xenografts had a tumor load of less than 5% of that found for Y79 or CSF-2 xenografts ($P < 0.05$). Conversely, all optic nerves of CSF-2 xenografts were positive for retinoblastoma and presented a tumor load 40 to 400 times higher than that observed in Y79 and HPG-12L xenografts, respectively, denoting the intrinsic capacity of this metastatic model to disseminate into the CNS.

Notably, RBG-1 xenografts were the only animals of which almost all (90%) presented tumor dissemination in the lymph nodes[22] (Supplementary Table S6). Finally, in all cases bone marrow specimens were negative for CRX mRNA.

After intracerebral (intraventricular) injection, CSF-2 and Y79 cells engrafted rapidly and the mice presented symp-

Investigative Ophthalmology & Visual Science

Downloaded from hwmaint.iovs.org on 04/26/2024

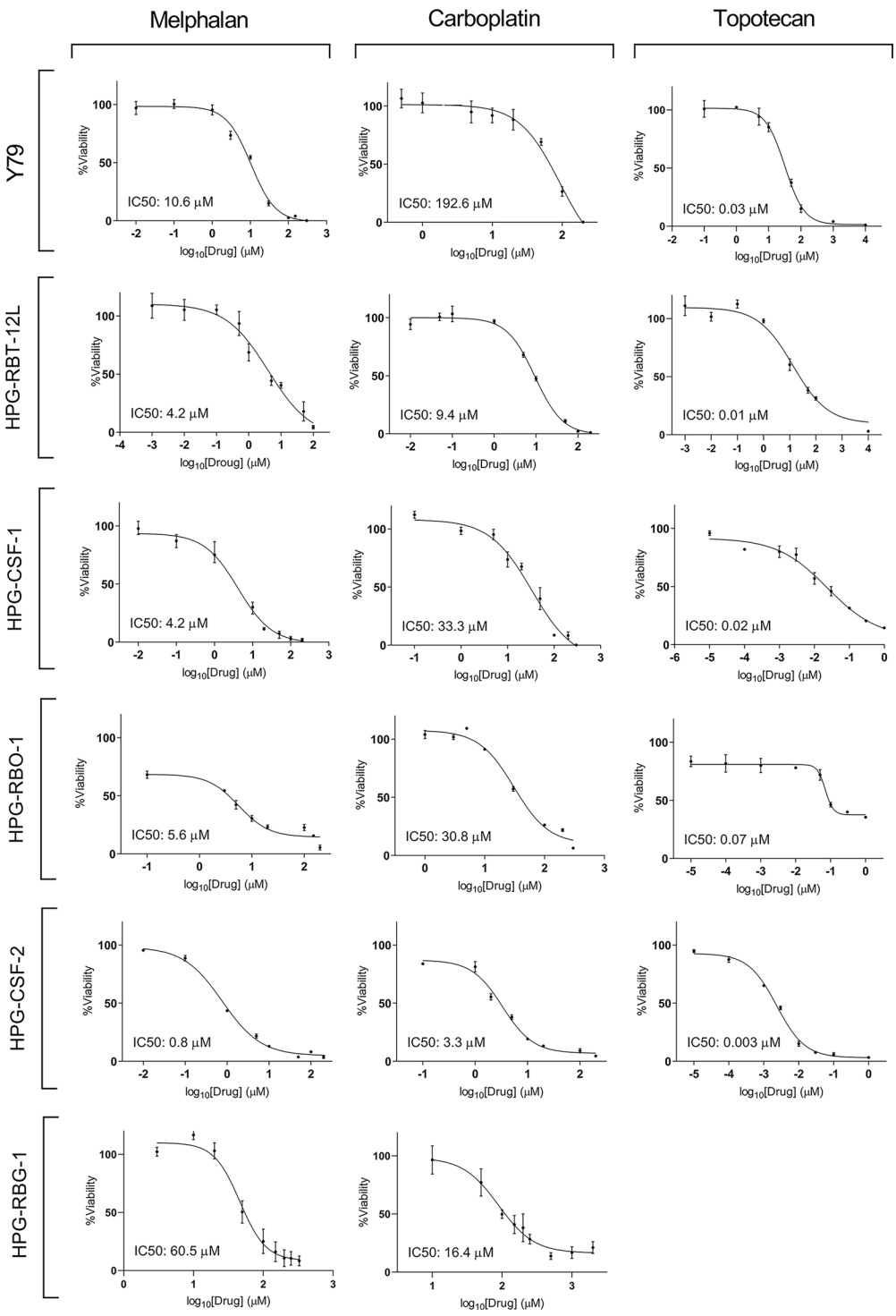

Figure 4. Drug sensitivity to common chemotherapy in primary cell lines. Tumor cell growth inhibition of standard-of-care agents in control and primary cell lines. Cell viability was determined at 72 hours using the methyl thiazole tetrazolium assay (MTT) assay. Symbols represent percentage of cell proliferation as compared to untreated control cells expressed as means (SEM) of three independent experiments. Data were fitted using a four-parameter nonlinear regression model.

toms of CNS disease, achieving a median overall survival (range) of 26 days (24–31) and 18 days (18–27), respectively (Fig. 5C). Histologically, intracerebral CSF-2 xenografts displayed tumor cells growing in an infiltrative pattern in the leptomeningeal space, parenchyma, and spinal cord (Fig. 5D). Conversely, intracerebral RBG-1 xenografts reached the experimental endpoint (45 days) without clinical signs of CNS disease and the histopathology showed absence of tumor engraftment in the CNS. These results are consistent with the clinical evolution of patient 7 who even in the end stages did not develop CNS tumor involvement (schematic representation in Fig. 1).

Investigative Ophthalmology & Visual Science

Downloaded from hwmaint.iovs.org on 04/26/2024

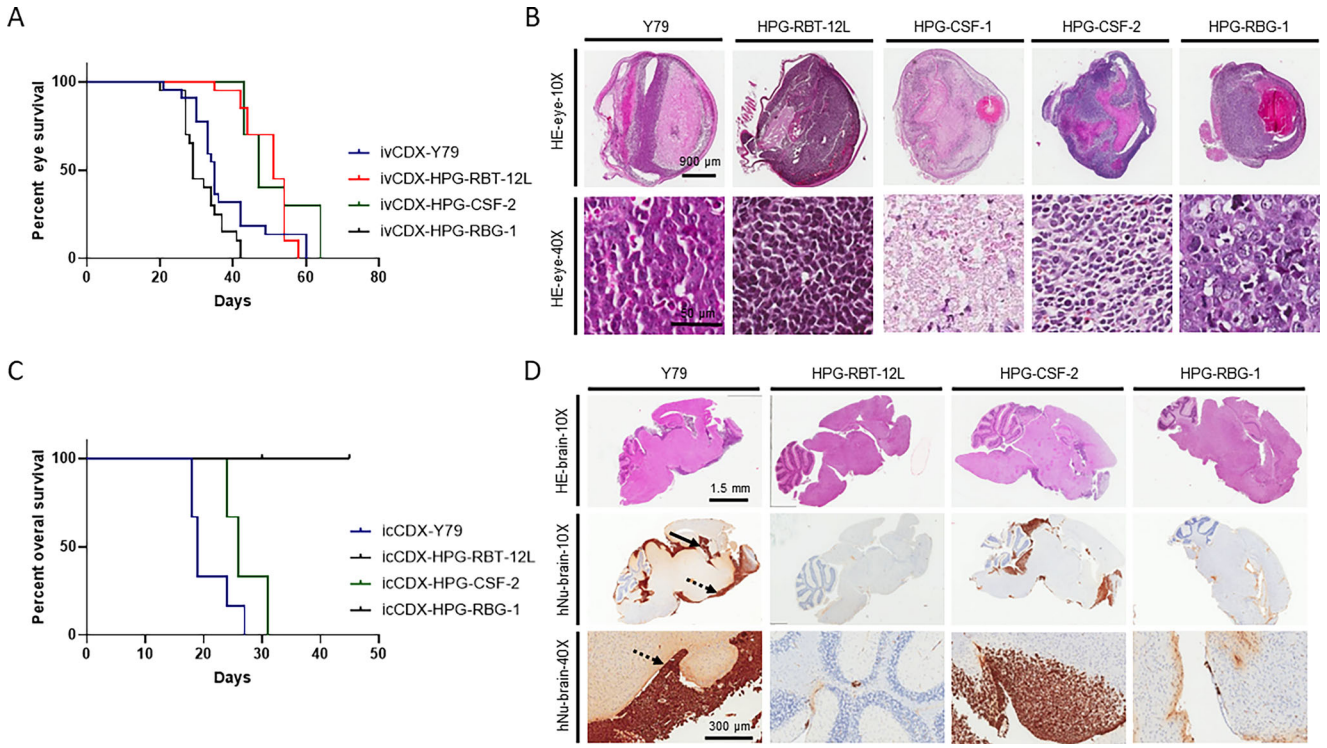

Figure 5. Survival curves and histopathologic features of intravitreal and intracerebral CDXs. (**A**) Eye survival curves of intravitreal CDXs. (**B**) Upper row, the hematoxylin-eosin (HE) stains are observed in the panoramic sections of the enucleated eyes of the established intravitreal tumor CDXs (×10), evidencing how the tumor occupies the entire ocular globe. In the case of the HPG-CSF-1 model, there was no evidence of intraocular tumor growth and areas of necrosis and calcium deposits were observed. The lower row (×40) shows that the histopathological characteristics of intravitreal HPG-RBT-12L cells resembled those of the enucleated eye of the patient,[49] whereas Y79 xenograft features were described elsewhere.[22,34] For HPG-CSF-2, a cellular morphology corresponding to medium-sized cells was observed, with a correct nucleus-cytoplasm ratio and without evident nucleoli. For the HPG-RGB-1 model, cells were large and anaplastic with hyperchromatic nuclei and prominent nucleoli. (**C**) Overall survival curves of intracerebral tumor CDX. (**D**) Tumor infiltration into the brain was assessed by: *Upper row* (×10), HE staining; middle and lower rows (×10 and ×40, respectively): anti-human nucleus (hNu) immunostaining. Y79 xenografts showed a large number of tumor cells located intraventricularly (*solid arrow*) and in the leptomeningeal space (*dotted arrow*) without an infiltrative pattern (*lower row*). HPG-CSF-2 xenografts showed the pattern of tumor invasion as Y79 but with infiltrative characteristics (*lower row*). HPG-RBT-12L and HPG-RBG-1 xenografts, in line with the absence of symptoms in the animals, these animals presented only small cell clusters without infiltration capacity (*lower row, brown stain*). Animals injected with the same cell culture showed the same pattern of infiltration and dissemination.

In line with the clinical and histological findings, molecular detection of retinoblastoma in the brains of intracerebral CSF-2 xenografts showed that all were positive and the tumor load was two and 200 times higher than that of the Y79 and HPG-12L xenografts, respectively (Supplementary Table S6). Although all brains of the intracerebral RBG-1 xenografts were positive for retinoblastoma, the tumor load was only 20% of that attained in Y79 xenografts, likely indicating the presence of only the inoculated tumor cells. Analysis of bone marrow samples showed that only animals that developed CNS symptoms (intracerebral Y79 and CSF-2 xenografts) were positive for tumor cells (3/6, 50% and 1/6, 16.6%, respectively) (Supplementary Table S6).

Discussion

We have developed and comprehensively characterized a unique preclinical platform of metastatic retinoblastoma as an essential tool for the understanding of the tumor biology of these aggressive tumors and for screening potential drug candidates to identify new treatment strategies. Our final aim is to leverage the information provided by the use of this platform to find new therapeutic interventions for patients who currently lack effective treatment options. Primary cell lines and xenografts accurately retained the histological and genomic features of the tumors from which they were derived and faithfully recapitulated the dissemination patterns and pharmacological sensitivity observed in the matched patients.

The incidence of metastatic retinoblastoma in Argentina has decreased over the last few decades.[35] Nevertheless, we enrolled seven patients in most of whom late diagnosis probably contributed to the development of metastasis. Although the cohort was small, the median age of the three unilateral patients with extraocular disease at diagnosis was 40 months. This results is in line with previous reports showing the association between lower income level, older age at presentation, and a higher proportion of metastatic disease.[9,36]

Expansion of human tumors in the flank of immunodeficient mice was successful in all cases but the bone marrow aspirate of one patient with hematogenous dissemination, probably due to the low tumor burden, which was insufficient for in vivo cell growth. In line with previous reports showing that the most aggressive pediatric tumors are the ones that engraft in mice and predict worse patient

Investigative Ophthalmology & Visual Science

Downloaded from hwmaint.iovs.org on 04/26/2024

outcomes,[14,37] all patients of our study died of their disease. Moreover, the xenograft with the fastest tumor growth was the one derived from the *MYCN* amplified *RB1*$^{+/+}$ tumor disseminated into the lymph node of patient 7 who died shortly after diagnosis despite intensive treatment.[22]

We developed four PDX models from metastatic cells that disseminated into the CSF (n = 3) and the orbit of four patients, as well as four primary cell lines derived from retinoblastoma dissemination in the CSF (CSF-1 and CSF-2), lymph node (RBG-1), and orbit (RBO-1). Importantly, we obtained models bearing genomic alterations in 11q, 17q, and 19q chromosomes that are more frequent in metastatic retinoblastoma and associated with aggressive features in neuroblastoma. All the primary cell lines present *MYCN* gains or amplification along with other genomic alterations including gains in 1q and 16q loss, which are particular features of subtype 2 tumors. This subtype was previously characterized as less differentiated, with stemness features and, importantly, with a higher frequency of metastases compared to subtype 1 tumors, as we observed in our cell models.[7] The concept that *MYCN* function confers an adaptive advantage to retinoblastoma cells is consistent with our observation that the only primary cells that did not grow in culture were those from patient 5, which had no 2p gain or amplification.[38–40] Nevertheless, we acknowledge that our data do not allow us to infer the clinical implications of *MYCN* amplification and an in-depth analysis of the effect of different levels of *MYCN* gain on the survival of the established cell lines is necessary. Altogether, we emphasize the importance of developing preclinical models bearing genomic alterations that are frequent in metastatic retinoblastoma to elucidate the molecular mechanisms associated with these alterations and to identify new therapies for a rationale management of high-risk patients.

We observed a close concordance between the metastatic cell lines and the matched tumor specimens in terms of genomic alterations and CNAs reported as drivers in retinoblastoma. A few differences were found in regions not previously recognized as relevant for the retinoblastoma phenotype or not harboring tumor suppressor or oncogenes. Overall, the similarities in the genomic profiles between tumors and the derived models validate the capacity of the established metastatic cell lines to resemble the matched tumor characteristics as appropriate research models.

The observation that RBG-1 cells exhibited the fastest growth was expected, given the aggressive behavior of the tumor in the matched patient and its low sensitivity to the most common chemotherapy used in retinoblastoma treatment.[22] This cell line is *MYCN* amplified and *TP53* mutant, which has been associated with a highly aggressive and chemoresistant phenotype in neuroblastoma.[41–43]

CSF-2 cells were collected from a chemotherapy-naïve patient, which partially accounts for their high sensitivity to the tested chemotherapy. Conversely, CSF-1 cells showed lower sensitivity to the evaluated agents, probably because of the development of acquired drug resistance in the heavily pretreated patient from whom they derive. Interestingly, RBO-1 cells derived from the orbital tumor of a chemotherapy-naïve patient showed similar or lower sensitivity to standard-of-care chemotherapy than that observed for CSF-2 cells. The longer doubling time leading to a reduced probability of targeting actively replicating cells by the cytotoxic agents may explain these findings.

The establishment of Y79 xenografts used as controls validated our workflow for in vivo assays.[21,34] The finding that most of the metastatic cells engrafted after intravitreal injection is superior to our previous experience in retinoblastoma xenografts established from intraocular tumors, in which approximately half of the models did not engraft.[21] However, it remains unclear why CSF-1 cells did not engraft in immunocompromised animals.

In animals intravitreally or intraventricularly injected with CSF-2 cells, the capacity of the xenografts to invade the brain parenchyma and subarachnoid space was retained, resembling the clinical course in the patient who rapidly died of leptomeningeal disease. In addition to the spatial continuity of the optic nerve and brain tissue, which could facilitate the dissemination of retinoblastoma cells into the CNS, the molecular characteristics of the tumors may also play an important role in CSF dissemination and should be elucidated. Despite the limited number of models of CSF dissemination that hinders unveiling the biological features of CSF-2 cells for homing to the CSF, our work in progress aims to identify novel routes of drug delivery targeting sanctuary tissues, such as the brain, and explore combinations of chemotherapy to prevent tumor dissemination in the SNC.

In our previous study, we showed that lymph node–derived RBG-1 xenografts faithfully resemble the pattern of tumor dissemination observed in the matched patient, with 100% tumor infiltration in the cervical lymph nodes of mice and none presenting CNS disease.[22] This patient had a highly aggressive and uncommon *RB1*$^{+/+}$ *MYCN*$_{ampl}$ retinoblastoma with mutated *TP53*. *TP53*, along with other mutated genes, has been proposed as driver of brain metastasis in adult tumors.[44] Intriguingly, the genomic profile of the *TP53*-mutated RBG-1 cell line, aggressive and probably induced after several rounds of chemotherapy, is more similar to that described for brain metastasis in adults than any other of the cell lines described in this study. However, contrary to those, the RBG-1 cells showed no capacity to invade CNS. Given the uniqueness of this cell line genomic profile, which has not been described in retinoblastoma, we can only speculate about the existence of inhibitory factors that prevent CNS homing. In this sense, published evidence involved miR-509 as a suppressor of brain metastasis in breast cancer.[45] Further studies should be performed to test this hypothesis.

Even more surprising was that the metastases of this model were limited to the lymph nodes, sparing the bone marrow. Further studies should be performed to delve into the molecular characteristics that may define a differential homing pathway in cases of lymph node invasion.

Distant metastasis to the bone marrow only developed in animals that had terminal CNS symptoms after intraventricular inoculation of cancer cells. This observation is in agreement with an important study in preclinical models of metastatic medulloblastoma. Garzia et al.[46] showed that distant metastasis to the bone marrow only developed in animals that had terminal CNS symptoms after intraventricular inoculation of cancer cells. Based on the observation of circulating tumor cells in genetically engineered animals and in an elegant model of medulloblastoma parabiosis, the investigators provided evidence that supports that upon inoculation in the mouse brain, medulloblastoma cells enter the blood circulation. Moreover, circulating medulloblastoma cells were proposed to disseminate, resulting in leptomeningeal metastases simultaneously to cell shedding from the primary tumor into the CSF. We speculate that similar mechanisms may be followed by retinoblas-

Investigative Ophthalmology & Visual Science

Downloaded from hwmaint.iovs.org on 04/26/2024

toma cells, in accordance with our observations.[46] Besides, extending the follow-up may have allowed tumor progression and hematogenous dissemination to reach quantifiable levels after intravitreal injection, but this was not ethically permissible.

Primary tumor cell lines play a crucial role in the identification of new treatment strategies for metastatic retinoblastoma. We previously reported on the use of CSF-1 cells to evaluate the sensitivity to anthracyclines, which are commonly used for advanced disease.[47] Also, we subjected some of the established primary cell lines to broad pharmacological testing evaluating thousands of compounds by means of high-throughput analysis and, subsequently, a drug decision process was developed to identify the most promising hits with potential for clinical translation.[48] For the highly resistant RBG-1 cells we found that the combination of bortezomib, panobinostat, and carboplatin significantly prolonged eye survival and prevented lymph node metastases in the animal model.[22]

We acknowledge certain limitations of our approach. First, biopsies are usually restricted to one spatial site and limited in amount and therefore may harvest subclonal populations that could not represent the whole tumor molecular characteristics. On the clinical side, small samples from metastatic retinoblastoma, such as orbital tumor biopsy specimens and cells in cerebrospinal fluid, require a first step of tumor expansion after subcutaneous engraftment in mice. This process results in a delay between sample collection and the evaluation of candidate agents, which may hinder an individualized pharmacological approach. Nevertheless, our main objective was to develop a rational decision-making process to define the most suitable treatment strategy for a group of patients with similar pharmacological sensitivity and clinical and genomic characteristics. This process should be validated in prospective clinical trials. Last, leaving aside patient 7 who had a unique genomic pattern and considering that all the other patients were classified as subtype 2, we could not find consistent genomic findings that may be associated with the phenotype characteristics of the developed model. Analysis of more cases in the future may contribute to unveiling the relations between genotype and phenotype in metastatic retinoblastoma.

Conclusions

Altogether, our novel preclinical platform effectively captured the phenotypic and biological heterogeneity of metastatic retinoblastoma. These models are unique tools to facilitate prioritization for testing the most promising drug candidates likely to be active in the clinical setting.

Acknowledgments

Analysis of RB1 mutations was performed in collaboration with Irene Szijan (Cátedra de Genética, Facultad de Farmacia y Bioquímica, Universidad de Buenos Aires. Buenos Aires, Argentina), whom we thank for her valuable contribution.

Supported by the National Agency for Science and Technology Promotion (PIDC 2014-0043); Fundación Leo Messi; Instituto Oncológico Henry Moore, Argentina; Fundación Natalie Dafne Flexer de Ayuda al Niño con Cancer, Argentina; Amazon Web Services Cloud Credits for Research; Foundation Nelia et Amadeo Barletta, Switzerland; Fund for Ophthalmic Knowledge, New York, NY, USA.

Author Contributions: Conceptualization: FR, DHA, ASLL, OP, GCH, AMC, PS.; Methodology: SZ, RA, DG, UW, DO, ASLL, OP, EGC, AMC, PS; Cell line establishment and phenotypical characterization: SZ, RA, MBC, UW, AT; Animal studies: SZ, RA, MBC, UW, AT, EGC, AMC; Histopathological and immunocytological evaluations: RA, GL, FL; Genomic analysis: DG, MM, ASLL, FR; Patient treatment and follow-up: CS, EL, MS, AF; Data analysis: SZ, RA, DG, MBC, UW, ASLL, PS; Writing: SZ, ASLL, PS; Funding acquisition: DHA, GCH, PS. All authors significantly contributed to the design of the study, data interpretation, writing and editing and agreed to the published version of the manuscript.

Disclosure: **S. Zugbi**, None; **R. Aschero**, None; **D. Ganiewich**, None; **M.B. Cancela**, None; **U. Winter**, None; **D. Ottaviani**, None; **C. Sampor**, None; **M. Dinardi**, None; **A.V. Torbidoni**, None; **M. Mena**, None; **L. Balaguer-Lluna**, None; **G. Lamas**, None; **M. Sgroi**, None; **E. Lagomarsino**, None; **F. Lubieniecki**, None; **A. Fandiño**, None; **F. Radvanyi**, None; **D.H. Abramson**, None; **O. Podhajcer**, None; **A.S. Llera**, None; **E.G. Cafferata**, None; **G. Chantada**, None; **A.M. Carcaboso**, None; **P. Schaiquevich**, None

References

1. Munier FL, Beck-Popovic M, Chantada GL, et al. Conservative management of retinoblastoma: challenging orthodoxy without compromising the state of metastatic grace. "Alive, with good vision and no comorbidity." *Progr Retin Eye Res*. 2019;73:100764.
2. Tomar AS, Finger PT, Gallie B, et al. Metastatic death based on presenting features and treatment for advanced intraocular retinoblastoma. *Ophthalmology*. 2022;129:933–945.
3. Tomar AS, Finger PT, Gallie B, et al. Global retinoblastoma treatment outcomes. *Ophthalmology*. 2021;128:740–753.
4. Tomar AS, Finger PT, Gallie B, et al. A multicenter, international collaborative study for American Joint Committee on Cancer Staging of Retinoblastoma. *Ophthalmology*. 2020;127:1719–1732.
5. Dunkel IJ, Khakoo Y, Kernan NA, et al. Intensive multimodality therapy for patients with stage 4a metastatic retinoblastoma. *Pediatr Blood Cancer*. 2010;55:55–59.
6. Aschero R, Francis JH, Ganiewich D, et al. Recurrent somatic chromosomal abnormalities in relapsed extraocular retinoblastoma. *Cancers (Basel)*. 2021;13(4):1–15.
7. Liu J, Ottaviani D, Sefta M, et al. A high-risk retinoblastoma subtype with stemness features, dedifferentiated cone states and neuronal/ganglion cell gene expression. *Nat Commun*. 2021;12(1):5578.
8. Rushlow DE, Mol BM, Kennett JY, et al. Characterisation of retinoblastomas without RB1 mutations: genomic, gene expression, and clinical studies. *Lancet Oncol*. 2013;14:327–334.
9. Fabian ID, Abdallah E, Abdullahi SU, et al. Global retinoblastoma presentation and analysis by national income level. *JAMA Oncol*. 2020;6:685–695.
10. Loh AHP, Stewart E, Bradley CL, et al. Combinatorial screening using orthotopic patient derived xenograft-expanded early phase cultures of osteosarcoma identify novel therapeutic drug combinations. *Cancer Lett*. 2019;442:262–270.
11. Stewart E, Federico SM, Chen X, et al. Orthotopic patient-derived xenografts of paediatric solid tumours. *Nature*. 2017;549(7670):96–100.
12. Atkinson JM, Shelat AA, Carcaboso AM, et al. An integrated in vitro and in vivo high-throughput screen identifies treatment leads for ependymoma. *Cancer Cell*. 2011;20:384–399.
13. Murphy AJ, Chen X, Pinto EM, et al. Forty-five patient-derived xenografts capture the clinical and biological heterogeneity of Wilms tumor. *Nat Commun*. 2019;10(1):5806.

Downloaded from hwmaint.iovs.org on 04/26/2024

14. Castillo-Ecija H, Pascual-Pasto G, Perez-Jaume S, et al. Prognostic value of patient-derived xenograft engraftment in pediatric sarcomas. *J Pathol Clin Res*. 2021; 7:338–349.
15. Brabetz S, Leary SES, Gröbner SN, et al. A biobank of patient-derived pediatric brain tumor models. *Nat Med*. 2018;24:1752–1761.
16. Inomata M, Kaneko A, Saijo N, Tokura S. Culture of retinoblastoma cells from clinical specimens: growth-promoting effect of 2-mercaptoethanol. *J Cancer Res Clin Oncol*. 1994;120:149–155.
17. Chantada G, Doz F, Antoneli CBG, et al. A proposal for an international retinoblastoma staging system. *Pediatr Blood Cancer*. 2006;47:801–805.
18. Winter U, Aschero R, Fuentes F, et al. Tridimensional retinoblastoma cultures as vitreous seeds models for live-cell imaging of chemotherapy penetration. *Int J Mol Sci*. 2019;20(5):1077.
19. Monje M, Mitra SS, Freret ME, et al. Hedgehog-responsive candidate cell of origin for diffuse intrinsic pontine glioma. *Proc Natl Acad Sci*. 2011;108:4453–4458.
20. Winter U, Mena HA, Negrotto S, et al. Schedule-dependent antiangiogenic and cytotoxic effects of chemotherapy on vascular endothelial and retinoblastoma cells. *PLoS One*. 2016;11(7):e0160094.
21. Pascual-Pasto G, Olaciregui NG, Vila-Ubach M, et al. Preclinical platform of retinoblastoma xenografts recapitulating human disease and molecular markers of dissemination. *Cancer Lett*. 2016;380(1):10–19.
22. Zugbi S, Ganiewich D, Bhattacharyya A, et al. Clinical, genomic, and pharmacological study of MYCN-amplified rb1 wild-type metastatic retinoblastoma. *Cancers (Basel)*. 2020;12(9):1–20.
23. Tschulakow AV, Schraermeyer U, Rodemann HP, Julien-Schraermeyer S. Establishment of a novel retinoblastoma (Rb) nude mouse model by intravitreal injection of human Rb Y79 Cells – comparison of in vivo analysis versus histological follow up. *Biol Open*. 2016;5:1625–1630.
24. Livak KJ, Schmittgen TD. Analysis of relative gene expression data using real-time quantitative PCR and the $2-\Delta\Delta CT$ method. *Methods*. 2001;25:402–408.
25. Ottaviani D, Alonso C, Szijan I. Uncommon RB1 somatic mutations in a unilateral retinoblastoma patient. *Medicina (B Aires)*. 2015;75:137–141.
26. DePristo MA, Banks E, Poplin R, et al. A framework for variation discovery and genotyping using next-generation DNA sequencing data. *Nat Genet*. 2011;43:491–498.
27. Edmonson MN, Patel AN, Hedges DJ, et al. Pediatric Cancer Variant Pathogenicity Information Exchange (PECANPIE): a cloud-based platform for curating and classifying germline variants. *Genome Res*. 2019;29:1555–1565.
28. Kopanos C, Tsiolkas V, Kouris A, et al. VarSome: the human genomic variant search engine. *Bioinformatics*. 2019;35:1978–1980.
29. Arora A, Shen R, Seshan VE. FACETS: fraction and allele-specific copy number estimates from tumor sequencing. *Methods Mol Biol*. 2022;493:89–105.
30. Lau JW, Lehnert E, Sethi A, et al. The Cancer Genomics Cloud: collaborative, reproducible, and democratized—a new paradigm in large-scale computational research. *Cancer Res*. 2017;77(21):e3–e6.
31. Li H, Durbin R. Fast and accurate short read alignment with Burrows-Wheeler transform. *Bioinformatics*. 2009;25:1754–1760.
32. Picard Tools - By Broad Institute Available at: http://broadinstitute.github.io/picard/. Accessed June 8, 2020.
33. Thériault BL, Dimaras H, Gallie BL, Corson TW. The genomic landscape of retinoblastoma: a review. *Clin Exp Ophthalmol*. 2014;42:33–52.
34. Chevez-Barrios P, Hurwitz MY, Louie K, et al. Metastatic and nonmetastatic models of retinoblastoma. *Am J Pathol*. 2000;157:1405–1412.
35. Moreno F, Sinaki B, Fandiño A, Dussel V, Orellana L, Chantada G. A population-based study of retinoblastoma incidence and survival in Argentine children. *Pediatr Blood Cancer*. 2014;61:1610–1615.
36. Mattosinho CCDS, Moura ATMS, Oigman G, Ferman SE, Grigorovski N. Time to diagnosis of retinoblastoma in Latin America: a systematic review. *Pediatr Hematol Oncol*. 2019;36:55–72.
37. Aschero R, Castillo-Ecija H, Baulenas-Farres M, et al. Prognostic value of xenograft engraftment in patients with metastatic high-risk neuroblastoma. *Pediatr Blood Cancer*. 2023;70(6):e30318.
38. Otte J, Dyberg C, Pepich A, Johnsen JI. MYCN function in neuroblastoma development. *Front Oncol*. 2021;10:624079.
39. Kang J-H, Rychahou PG, Ishola TA, Qiao J, Evers BM, Chung DHM. Silencing induces differentiation and apoptosis in human neuroblastoma cells. *Biochem Biophys Res Commun*. 2006;351:192–197.
40. Blixt MKE, Hellsand M, Konjusha D, et al. MYCN induces cell-specific tumorigenic growth in RB1-proficient human retinal organoid and chicken retina models of retinoblastoma. *Oncogenesis*. 2022;11(1):34.
41. Xue C, Haber M, Flemming C, et al. P53 determines multidrug sensitivity of childhood neuroblastoma. *Cancer Res*. 2007;67:10351–10360.
42. Keshelava N, Zuo JJ, Chen P, et al. Loss of P53 function confers high-level multidrug resistance in neuroblastoma cell lines. *Cancer Res*. 2001;61:6185–6193.
43. Chen L, Esfandiari A, Reaves W, et al. Characterisation of the P53 pathway in cell lines established from TH-MYCN transgenic mouse tumours. *Int J Oncol*. 2018;52:967–977.
44. Campbell BK, Gao Z, Corcoran NM, Stylli SS, Hovens CM. Molecular mechanisms driving the formation of brain metastases. *Cancers (Basel)*. 2022;14:4963.
45. Xing F, Sharma S, Liu Y, et al. MiR-509 suppresses brain metastasis of breast cancer cells by modulating RhoC and TNF α. *Oncogene*. 2015;34:4890.
46. Garzia L, Kijima N, Morrissy AS, et al. A hematogenous route for medulloblastoma leptomeningeal metastases. *Cell*. 2018;172:1050–1062.e14.
47. Zugbi S, Winter U, Castañon A, Sampor C, Chantada G, Schaiquevich P. Comparison of the pharmacological activity of idarubicin and doxorubicin for retinoblastoma. *Pediatr Blood Cancer*. 2019;66(1):e27441.
48. Cancela MB, Zugbi S, Winter U, et al. A decision process for drug discovery in retinoblastoma. *Invest New Drugs*. 2021;39:426–441.
49. Winter U, Ganiewich D, Ottaviani D, et al. Genomic and transcriptomic tumor heterogeneity in bilateral retinoblastoma. *JAMA Ophthalmol*. 2020;138:569–574.
50. Pérez V, Sampor C, Rey G, et al. Treatment of nonmetastatic unilateral retinoblastoma in children. *JAMA Ophthalmol*. 2018;136:747–752.
51. Rodriguez A, Zugbi S, Requejo F, et al. Combined high-dose intra-arterial and intrathecal chemotherapy for the treatment of a case of extraocular retinoblastoma. *Pediatr Blood Cancer*. 2018;65(12):e27385.

Investigative Ophthalmology & Visual Science

Downloaded from hwmaint.iovs.org on 04/26/2024